Design of Compact Arbitrary-Ratio Multimode Power Splitters Based on Topological Derivative

Julián L. Pita Ruiz, Ivan Aldaya, *Member, IEEE*, Paulo Dainese, and Lucas H. Gabrielli, *Member, IEEE*

***Abstract*— Compact unbalanced splitters are a key constitutive block to achieve flexibility in future multimode applications relying on silicon-on-insulator technology. Their design, however, poses significant challenges as it has to combine high performance for the different supported modes, a compact size, and compliance with fabrication constraints. In this letter, we employ topological derivative to optimize the design of bimodal unbalanced splitters with predefined split ratios of 2:1 and 3:1. Numerical simulations reveal that the optimized devices achieve the desired ratios with insertion losses of 0.6 dB and 0.5 dB, and crosstalks of −18.2 dB and −16.4 dB, both in a compact footprint of 4.2 μm × 3.5 μm.**

***Index Terms*— Silicon photonics, integrated optics, mode division multiplexing.**

I. Introduction

DUE to its compatibility with complementary metal-oxide-semiconductor (CMOS) manufacturing, a silicon-on-insulator (SOI) platform has emerged as a solution to the integration between electronic signal processing and the optical front/back-end [1], [2]. Although most integrated photonic circuits rely on single-mode waveguides and devices, mode division multiplexing can be exploited to improve overall throughput or to improve the performance of optical signal processing by means of parallelization [3], [4]. In this context, there is an increasing effort to design and improve multi-mode building blocks that can be interconnected to meet the most diverse applications. For example, in [5]–[8] different mode multiplexers are reported, whereas in [9], [10] and in [11]–[14], multi-mode waveguides crossing and bendings are presented, respectively. Balanced splitters have also been a research subject [15]–[17]. Unbalanced splitters, nevertheless, have been little explored, being limited to single-mode operation [18] or to devices with extremely large areas [19]. These are however critical components for many applications ranging from signal strength monitoring to flexible power distribution networks. In particular, unbalanced splitters are required for general networks with an arbitrary number of outputs and optical phased arrays with optimized element weights.

The design of multi-mode devices is complex, because it has to combine small footprint and high performance for the different supported modes simultaneously. Such requirements can hardly be achieved by analytical methods and end up requiring optimization algorithms that typically result in non-intuitive designs. Methods based on topological optimization are particularly interesting as they make use of the knowledge of the cost function and its derivatives, which significantly reduces the number of iterations to achieve satisfactory results. Several approaches have been successfully demonstrated in recent years. For instance, pixel optimization is proposed in [20], an objective-first optimization method is developed and analyzed in [21], and in [22], the optimization is addressed by a density-based method. More recently, a method based on the topological derivative was introduced in [23], which is particularly attractive due to its straightforward implementation and because it can easily implement multiple etch levels present in SOI devices.

In this letter, we employ the aforementioned topological derivative-based optimization method to design two unbalanced bimodal splitters with split ratios (SRs) of 2:1 and 3:1, corresponding to power distributions of 67% to 33% and 75% to 25%, respectively. Numerical results show that the insertion loss (IL) in the band from 1.5 μm to 1.6 μm remains below 1.3 dB, while the crosstalk (XT) is lower than −12.2 dB in both cases. These results are achieved in devices with footprint areas of 4.2 μm × 3.5 μm, representing, to the best of our knowledge, the smallest unballanced multimode splitters to date.

Manuscript received May 28, 2020; revised July 16, 2020; accepted August 9, 2020. Date of publication August 12, 2020; date of current version August 24, 2020. This work was supported in part by the National Council for Scientific and Technological Development (CNPq) under Grant 302036/2018-0, Grant 311035/2018-3, and Grant 432303/2018-9, in part by the São Paulo Research Foundation (FAPESP) under Grant 2015/24517-8, Grant 2016/19270-6, and Grant 2018/25339-4, and in part by the Coordenação de Aperfeiçoamento de Pessoal de Nível Superior (CAPES), through the Program Capes-PrInt 2837/2018. *(Corresponding author: Julián L. Pita Ruiz.)*

Julián L. Pita Ruiz is with the School of Electrical and Computer Engineering, University of Campinas, Campinas 13083-859, Brazil, also with the Quantum Electronics Department, Gleb Wataghin Physics Institute, University of Campinas, Campinas 13083-859, Brazil, and also with the Photonics Research Center, University of Campinas, Campinas 13083-859, Brazil (e-mail: jpita@unicamp.br).

Ivan Aldaya is with the Campus of São João da Boa Vista, State University of São Paulo, São João da Boa Vista 13876-750, Brazil, and also with the Photonics Research Center, University of Campinas, Campinas 13083-859, Brazil.

Paulo Dainese is with Corning Research and Development Corporation, One Science Drive, Corning, NY 14830, USA, also with the Quantum Electronics Department, Gleb Wataghin Physics Institute, University of Campinas, Campinas 13083-859, Brazil, and also with the Photonics Research Center, University of Campinas, Campinas 13083-859, Brazil.

Lucas H. Gabrielli is with the School of Electrical and Computer Engineering, University of Campinas, Campinas 13083-852, Brazil, and also with the Photonics Research Center, University of Campinas, Campinas 13083-859, Brazil.

Color versions of one or more of the figures in this letter are available online at http://ieeexplore.ieee.org.

Digital Object Identifier 10.1109/LPT.2020.3016012

1041-1135 © 2020 IEEE. Personal use is permitted, but republication/redistribution requires IEEE permission.
See https://www.ieee.org/publications/rights/index.html for more information.

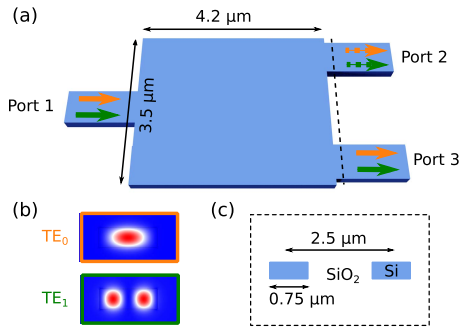

Fig. 1. Optimization scenario including (a) the optimization region with input and output multimode waveguides, (b) the mode profiles of the two TE modes, and (c) a cross-section view from the cut at the dashed line. The colors of the input and output arrows indicate the mode at the port. At the output, dashed and continuous arrows represent waveguides 1 and 2, respectively. Both colors and formats are kept along the work to make the data interpretation easier.

II. Optimization of SoI Devices Employing Topological Derivative

Our goal is to design a compact splitter to divide unevenly the power of the first two TE modes supported by the waveguide: TE_0 and TE_1, shown in Fig. 1. The target SR is the same for both modes. The optimization region is an area of 4.2 μm $\times$ 3.5 μm with one input port and two output ports waveguides. All waveguides have a width of 750 nm and a 250 nm-thick silicon layer. The input port is centered on one of the minor sides of the optimization region and the outputs ports are separated by 2.5 μm (center-to-center) on the opposite side. All surrounding regions are assumed to be silicon dioxide. In order to simplify fabrication, the optimization algorithm was configured to produce only un-etched or fully-etched regions, as well as ensure a minimum feature size of 60 nm.

The error function minimized in the optimization process is described by:

$$\mathcal{E} = \sum_{\lambda} \sum_{m=1}^{2} \sum_{\ell=2}^{3} \left(T_{\ell m} - |S_{\ell m}(\lambda)|^2 \right)^2 \tag{1}$$

in which $T_{\ell m}$ is the target transmission coefficient for port ℓ and mode m, $S_{\ell m}$ is the respective scattering parameter calculated through the overlap integral, and the summation in λ runs over the wavelengths at which the optimization is performed, namely 1.53 μm and 1.57 μm.

The optimization region is uniformly initialized with silicon dioxide. At each iteration, both the direct and adjoint electromagnetic problems are solved using Comsol Multiphysics. The combined solutions are employed in the calculation of the topological derivative of the error function and used in a gradient descent method. A detailed description of the topological derivative calculation and the optimizations method can be found in [23]. The 2:1 and 3:1 splitters were optimized in a 2 GHz, 8-core cluster, and required 42 and 43 iterations to converge, respectively. Figures 2(a) and 3(a) show the final designs. It is clear that both structures converge to asymmetrical Y-branches with specific features that produce the desired power SRs. As designed, the devices can be fabricated in a single etch step of 250 nm and are free of small holes or islands (all features are larger than 60 nm).

III. Numerical Results

The Lumerical 3d finite-difference in time-domain solver was used to assess the performance of the optimized splitters in a broader wavelength window from 1.5 μm to 1.6 μm. The simulation domain was configured to include a silicon substrate, a buried oxide layer of 3 μm, a silicon layer of 250 nm, and a silica cladding of 1.5 μm. The designs were evaluated in terms of the power SR between output ports for each mode independently, the IL for each mode and each output port (with respect to the nominal power level), and the modal XT for each incident mode. In all cases, the power of each mode was calculated by the overlap integral between the total field distribution and the desired mode. Since the SR is one of the main performance metrics for unbalanced splitters, we define the operation bandwidth of the device as the range of wavelengths where the SR variation is below 10% (considering the narrowest among the two modes).

In Fig. 2(a-f), we show the numerical results for the 2:1 splitter. The top view of the device is depicted in Fig. 2(a), representing in grey and white the regions filled with silicon and silicon dioxide, respectively. The SR is presented in Fig. 2(b), which shows that it remains close to the nominal value of 2 for the whole simulation band. The largest deviation occurs at shorter wavelengths, where the SR for the TE_0 rises up to 2.28 and for the TE_1 decreases to 1.77. The 10% error bandwidth for TE_0 and TE_1 are, respectively, 84 nm and 86 nm. Plots of field intensities and power coupling efficiencies for both modes and output ports are presented in Figs. 2(c–f). In particular, Figs. 2(c) and (e) present the electric field intensity for each incident mode at 1.55 μm. They show the unbalanced power division between both output ports and minimum scattered or reflected power throughout the device, which contributes to the low IL. The existence of some XT can be noted by the slightly distorted field profiles at the outputs, even though the exact values are well below -15 dB. The coupling efficiency and the XT are quantified in Figures 2(d) and (f) for TE_0 and TE_1, respectively. Throughout the whole simulation band, the IL does not exceed 1.2 dB and the modal XT remains below -14.8 dB.

Figs. 3(a-f) are analogous to Figs. 2(a-f), but for the 3:1 splitter. Similar conclusions regarding SR, IL, and modal XT can be drawn for this device as for the 2:1 splitter. Quantitatively, the 3:1 splitter presents a narrower bandwidth of 63 nm; all three figures of merit worsen sooner as the wavelength departs from 1.55 μm. Nonetheless, the IL and modal XT are still at a maximum 1.3 dB and -12.2 dB, respectively, in the full simulated wavelength range. There is a trade-off between performance and occupied area, and one might explore larger devices for applications that require ultra-low insertion loss. In comparison to related designs, both the 2:1 and 3:1 splitters present insertion loss in the range of 1 dB to 1.5 dB reported for the unbalanced single-mode [18] and balanced multi-mode splitters [17]. Regarding bandwidth, the designs presented here can operate in a broader band

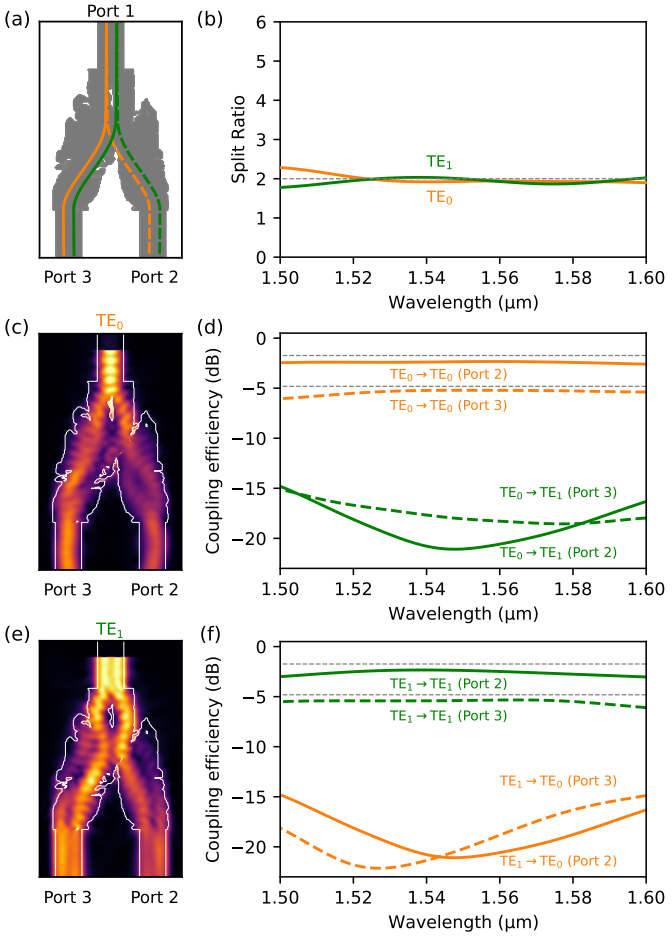

Fig. 2. Numerical characterization of the optimized 2:1 splitter. (a) Top view of the 2:1 optimized splitter. (b) SR as a function of the wavelength for each design. (c) Electric field intensity for TE_0 input. (d) Power coupling efficiencies for TE_0 input. (e) Electric field intensity for TE_1 input. (f) Power coupling efficiencies for TE_1 input. Continuous and dashed lines correspond to the mode coupling at ports 2 and 3, respectively, whereas the color is associated with the output mode: orange for TE_0 and green for TE_1. Dashed grey lines represent the target values.

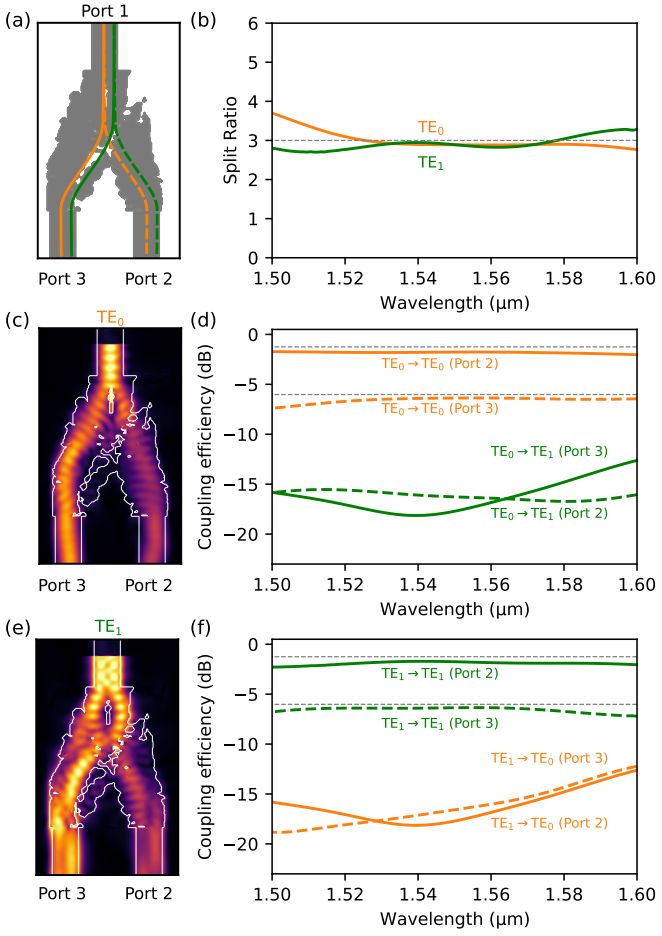

Fig. 3. Numerical characterization of the optimized 3:1 splitter. (a) Top view of the 3:1 optimized splitter. (b) SR as a function of the wavelength for each design. (c) Electric field intensity for TE_0 input. (d) Power coupling efficiencies for TE_0 input. (e) Electric field intensity for TE_1 input. (f) Power coupling efficiencies for TE_1 input. Continuous and dashed lines correspond to the mode coupling at ports 2 and 3, respectively, whereas the color is associated with the output mode: orange for TE_0 and green for TE_1. Dashed grey lines represent the target values.

than those reported in [17], [18]. Compared to the compact balanced multi-mode splitter in [17], the modal XT is similar for the 2:1 splitter, while slightly worse for the 3:1 splitter. On the other hand, although the multimode unbalanced splitter in [19] presents better performance in terms of IL, bandwidth, and XT, its footprint is 35 times larger than the area occupied by the devices in this work, a key metric for large-scale integration.

In order to evaluate the fabrication feasibility, we simulated the device after modifying the design to account for under-corrosion/over-exposure and over-corrosion/under-exposure. These effects were emulated applying erosion and dilation filtering corresponding to a 20 nm variation. As can be seen in Fig. 4(a), for the 2:1 splitter both operations affect the two modes in a similar way, dilation being the most harmful specially at short wavelengths. Regarding the 3:1 splitter, erosion affects similarly to both modes but the impact of dilation is more notorious for the TE_1 than for TE_0. In fact, dilation makes the SR to significantly diverge, exceeding a value of 4 for a wavelength of 1.51 μm. In both splitters,

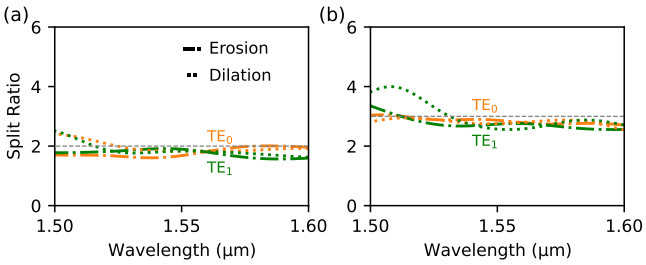

Fig. 4. Analysis of sensitivity to fabrication imperfections for (a) 2:1 and (b) 3:1 splitters. Dot-line curves indicate the results for erosion and dotted lines for dilation. Regarding the modes, the results for TE_0 and TE_1 are represented by orange and green, respectively.

the fabrication imperfections have a minimal effect on the SR at 1.55 μm but they lead to a bandwidth reduction of 46 nm and 40 nm, for the 2:1 and 3:1 splitters, respectively.

IV. Conclusion

In this letter, we presented two compact multimode unbalanced splitters with predefined SRs of 2:1 and 3:1.

The devices were designed using a topological derivative-based optimization method, which allows us to achieve the desired SR with low IL and XT in the band ranging from 1.5 μm to 1.6 μm, while keeping a footprint area as small as 4.5 μm $\times$ 3.2 μm. At the central operation wavelength of 1.55 μm, simulations reveal that the 2:1 splitter presents IL of 1.2 dB and modal XT of -14.8 dB. Similarly, the 3:1 splitter achieves IL of 1.3 dB and modal XT of -12.2 dB. These numbers represent, to the best of acknowledge, the most compact unbalanced multimode splitters for silicon photonics.

REFERENCES

[1] D. Thomson *et al.*, "Roadmap on silicon photonics," *J. Opt.*, vol. 18, no. 7, p. 073003, 2016.

[2] Y. Shen *et al.*, "Silicon photonics for extreme scale systems," *J. Lightw. Technol.*, vol. 37, no. 2, pp. 245–259, Jan. 15, 2019.

[3] X. Wu, C. Huang, K. Xu, W. Zhou, C. Shu, and H. K. Tsang, "3×104 Gb/s single-λ interconnect of mode-division multiplexed network with a multicore fiber," *J. Lightw. Technol.*, vol. 36, no. 2, pp. 318–324, Jan. 15, 2018.

[4] Y. Hsu *et al.*, "2.6 Tbit/s on-chip optical interconnect supporting Mode-Division-Multiplexing and PAM-4 signal," *IEEE Photon. Technol. Lett.*, vol. 30, no. 11, pp. 1052–1055, Jun. 1, 2018.

[5] L. F. Frellsen, Y. Ding, O. Sigmund, and L. H. Frandsen, "Topology optimized mode multiplexing in silicon-on-insulator photonic wire waveguides," *Opt. Express*, vol. 24, no. 15, pp. 16866–16873, 2016.

[6] K. Wang, X. Ren, W. Chang, L. Lu, D. Liu, and M. Zhang, "Inverse design of digital nanophotonic devices using the adjoint method," *Photon. Res.*, vol. 8, no. 4, pp. 528–533, 2020.

[7] L. Xu *et al.*, "Ultra-broadband and compact two-mode multiplexer based on Subwavelength-Grating-Slot-Assisted adiabatic coupler for the Silicon-on-Insulator platform," *J. Lightw. Technol.*, vol. 37, no. 23, pp. 5790–5800, Dec. 1, 2019.

[8] H. Xie *et al.*, "Highly compact and efficient four-mode multiplexer based on pixelated waveguides," *IEEE Photon. Technol. Lett.*, vol. 32, no. 3, pp. 166–169, Feb. 1, 2020.

[9] W. Chang *et al.*, "An ultracompact multimode waveguide crossing based on subwavelength asymmetric Y-junction," *IEEE Photon. J.*, vol. 10, no. 4, pp. 1–8, Aug. 2018.

[10] Y. Liu *et al.*, "Arbitrarily routed mode-division multiplexed photonic circuits for dense integration," *Nature Commun.*, vol. 10, no. 1, pp. 1–7, Dec. 2019.

[11] H. Wu, C. Li, L. Song, H.-K. Tsang, J. E. Bowers, and D. Dai, "Ultra-sharp multimode waveguide bends with subwavelength gratings," *Laser Photon. Rev.*, vol. 13, no. 2, Feb. 2019, Art. no. 1800119.

[12] H. Xie, Y. Liu, Z. Chu, K. Xu, J. Du, and Q. Song, "Ultra-compact dual-mode waveguide bend based on an inverse design," in *Proc. Int. Photon. Optoelectron. Meeting (POEM)*, 2018, p. OT4A-30.

[13] C. Sun, Y. Yu, G. Chen, and X. Zhang, "Ultra-compact bent multimode silicon waveguide with ultralow inter-mode crosstalk," *Opt. Lett.*, vol. 42, no. 15, pp. 3004–3007, 2017.

[14] S. Li *et al.*, "Universal multimode waveguide crossing based on transformation optics," *Optica*, vol. 5, no. 12, pp. 1549–1556, 2018.

[15] Y. Luo, Y. Yu, M. Ye, C. Sun, and X. Zhang, "Integrated dual-mode 3 dB power coupler based on tapered directional coupler," *Sci. Rep.*, vol. 6, no. 1, p. 23516, Sep. 2016.

[16] W. Chang *et al.*, "Inverse design and demonstration of an ultracompact broadband dual-mode 3 dB power splitter," *Opt. Express*, vol. 26, no. 18, pp. 24135–24144, 2018.

[17] H. Xie *et al.*, "An ultra-compact 3-dB power splitter for three modes based on pixelated meta-structure," *IEEE Photon. Technol. Lett.*, vol. 32, no. 6, pp. 341–344, Mar. 15, 2020.

[18] K. Xu *et al.*, "Integrated photonic power divider with arbitrary power ratios," *Opt. Lett.*, vol. 42, no. 4, pp. 855–858, Feb. 2017.

[19] H. Xu, D. Dai, and Y. Shi, "Ultra-broadband on-chip multimode power splitter with an arbitrary splitting ratio," *OSA Continuum*, vol. 3, no. 5, pp. 1212–1221, 2020.

[20] X. Ren, W. Chang, L. Lu, M. Yan, D. Liu, and M. Zhang, "Digitized adjoint method for inverse design of digital nanophotonic devices," 2019, *arXiv:1902.00654*. [Online]. Available: http://arxiv.org/abs/1902.00654

[21] L. Su, D. Vercruysse, J. Skarda, N. V. Sapra, J. A. Petykiewicz, and J. Vučković, "Nanophotonic inverse design with SPINS: Software architecture and practical considerations," *Appl. Phys. Rev.*, vol. 7, no. 1, Mar. 2020, Art. no. 011407.

[22] J. S. Jensen and O. Sigmund, "Topology optimization for nano-photonics," *Laser Photon. Rev.*, vol. 5, no. 2, pp. 308–321, Mar. 2011.

[23] J. L. P. Ruiz, A. A. Amad, L. H. Gabrielli, and A. A. Novotny, "Optimization of the electromagnetic scattering problem based on the topological derivative method," *Opt. Express*, vol. 27, no. 23, pp. 33586–33605, 2019.